Journal of Molecular Liquids 213 (2016) 122–138

Contents lists available at ScienceDirect

Journal of Molecular Liquids

journal homepage: www.elsevier.com/locate/molliq

Electrochemical, thermodynamic and quantum chemical studies of synthesized benzimidazole derivatives as corrosion inhibitors for N80 steel in hydrochloric acid

M. Yadav [a,*], S. Kumar [a], T. Purkait [a], L.O. Olasunkanmi [b], I. Bahadur [b,*], E.E. Ebenso [b]

[a] Department of Applied Chemistry, Indian School of Mines, Dhanbad 826004, India
[b] Department of Chemistry, School of Mathematical and Physical Sciences, Materials Science Innovation & Modelling (MaSIM) Research Focus Area, Faculty of Agriculture, Science and Technology, North-West University (Mafikeng Campus), Private Bag X2046, Mmabatho 2735, South Africa

ARTICLE INFO

Article history:
Received 10 July 2015
Received in revised form 26 September 2015
Accepted 8 November 2015
Available online xxxx

Keywords:
N80 steel
Hydrochloric acid
Corrosion inhibition
EIS
SEM
DFT

ABSTRACT

The inhibitive action of synthesized benzimidazole derivatives, namely: 2-(1-(morpholinomethyl)-1*H*-benzo[*d*]imidazol-2-yl)phenol (MBP), 2-(1-((piperazine-1-yl)methyl)-1*H*-benzo[*d*]imidazol-2-yl)phenol (PzMBP) and 2-(1-((piperidine-1-yl)methyl)-1*H*-benzo[*d*]imidazol-2-yl)phenol (PMBP) on corrosion of N80 steel in 15% HCl solution has been studied using weight loss measurement, potentiodynamic polarization and electrochemical impedance spectroscopy (EIS) techniques. It was found that the inhibition efficiency of all the three inhibitors increases with increase in concentration of inhibitors and decreases with increase in temperature. The inhibitors, PzMBP, MBP, and PMBP show corrosion inhibition efficiency of 96.3, 94.4 and 92.9% respectively, at 200 ppm and 303 K. Polarization studies showed that the studied inhibitors are mixed type in nature. The results of the Fourier transform infrared (FTIR) and UV–visible spectroscopy provided evidence of iron/inhibitors interactions. Scanning electron microscopy (SEM) and atomic force microscopy (AFM) were performed for surface analysis of N80 steel samples in acid solution without and with inhibitors. The Density Functional Theory (DFT) was employed for quantum chemical calculations to correlate the experimental findings.

1. Introduction

Carbon steel is widely used as constructional material in a large number of industries. N80 steel is widely used as main constructional material for down-hole tubular, casings, flow lines and transmission pipelines in petroleum industry. Acid solutions widely used in various industrial processes such as oil-well acidizing, acid pickling, industrial acid cleaning and acid descaling lead to serious metallic corrosion. Acidification of petroleum oil-well for enhanced oil production is commonly carried out by forcing a solution of 15% to 28% hydrochloric acid solution [1–8] into the oil-well through N80 tubing. During this process tubing and casing materials (N80 steel) get adversely affected by corrosion. In order to reduce the aggressive attack of the acid on tubing and casing materials (N80 steel), inhibitors are added to the acid solution during the acidifying process. The use of inhibitors is one of the most economical and practical methods of reducing corrosive attack on metals. The selection of inhibitor is controlled by its economic availability, its efficiency to inhibit the substrate material and its environmental side effects. Most of the inhibitors for corrosion of steel in acidic medium are organic compound containing nitrogen, oxygen and/or sulfur atoms [9–13]. The inhibiting action of these compounds is usually due to their adsorption onto the metal interface. The adsorption process depends upon the nature and surface charge of the metal, the type of aggressive media, the electronic and/or molecular structure of the inhibitor and the nature of its interaction with the metal surface [14].

Most of the reported organic corrosion inhibitors are effective only at high concentrations and are harmful to the environment due to their toxicity. Hence, it is important to search for new nontoxic and effective organic corrosion inhibitors for N80 steel in 15% hydrochloric acid. Some benzimidazole derivatives [15–19] have been reported as good inhibitors for the corrosion of metals and alloys in hydrochloric acid solution and their inhibition performance is influence by the nature and position of substituent groups on the aromatic rings. In addition to their good corrosion inhibition potentials, benzimidazole derivatives exhibit good solubility, high stability, and lower toxicity [20], which are among the other desirable characteristics often considered in selecting corrosion inhibitors.

In continuation of our research for developing organic compounds with high corrosion inhibition efficiency [5–8], the present paper explores the synthesis of three benzimidizole derivatives, namely, 2-(1-(morpholinomethyl)-1*H*-benzo[*d*]imidazol-2-yl)phenol (MBP), 2-(1-((piperazine-1-yl)methyl)-1*H*-benzo[*d*]imidazol-2-yl)phenol (PzMBP)

* Corresponding authors.
E-mail addresses: yadavdrmahendra@yahoo.co.in (M. Yadav), bahadur.indra@gmail.com (I. Bahadur).

http://dx.doi.org/10.1016/j.molliq.2015.11.018
0167-7322/

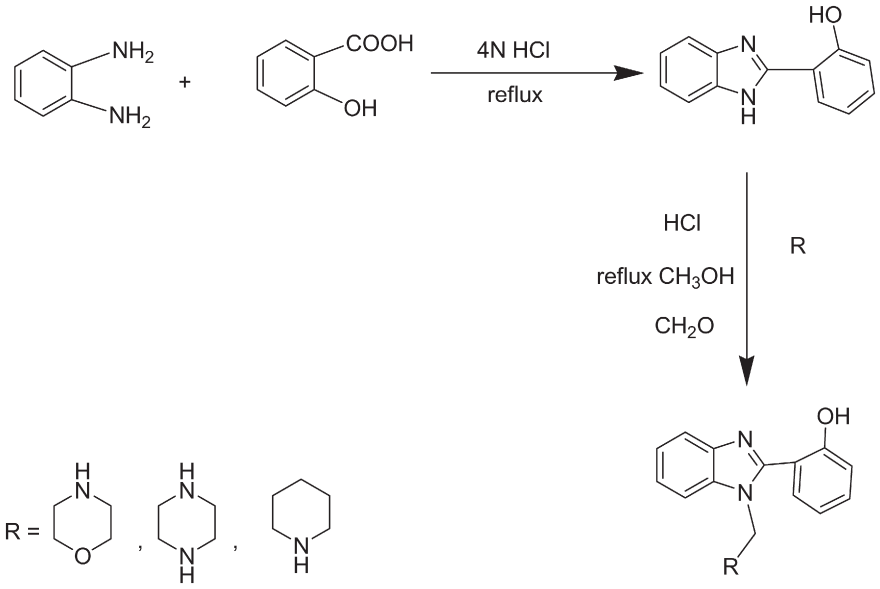

Scheme 1. Synthetic route of inhibitors PzMBP, MBP and PMBP.

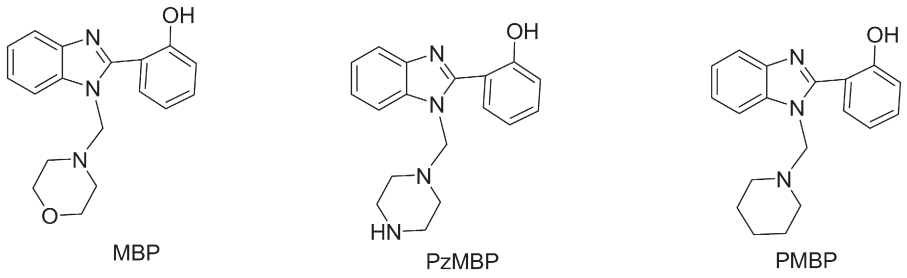

Fig. 1. Structure of inhibitors PzMBP, MBP and PMBP.

and 2-(1-((piperidine-1-yl)methyl)-1*H*-benzo[*d*]imidazol-2-yl)phenol (PMBP), and the systematic study of their inhibitive actions on the corrosion of N80 steel in 15% HCl solution using weight loss measurements, potentiodynamic polarization, AC impedance, FTIR, UV–visible spectroscopy, SEM, AFM and quantum chemical calculations. The structures of the studied compounds are similar and only differ in the group attached to the N1 atom on benzimidazole ring such that PzMBP contains piperazine ring, MBP contains morpholine ring whereas PMBP contains piperidine ring. The effect of different substituents attached to the N1 atom of benzimidazole ring on the corrosion inhibition properties of

Table 1
Corrosion parameters obtained from weight loss measurements of N80 steel in 15% HCl solution in the presence and absence of inhibitors at different temperatures.

Conc. (M)	303 K			313 K			323 K			333 K		
	CR (mmy^{-1})	θ	η%	*CR* (mmy^{-1})	θ	η%	*CR* (mmy^{-1})	θ	η%	*CR* (mmy^{-1})	θ	η%
Blank	20.20	–	–	34.55	–	–	55.47	–	–	92.69	–	–
PzMBP												
6.46×10^{-5} M	3.89	0.80	80.7	7.39	0.78	78.6	13.51	0.75	75.6	25.85	0.72	72.1
16.1×10^{-5} M	2.80	0.86	86.1	5.48	0.84	84.1	10.38	0.81	81.2	20.33	0.78	78.0
32.3×10^{-5} M	1.88	0.90	90.6	3.87	0.89	88.8	7.67	0.86	86.1	15.64	0.83	83.1
48.5×10^{-5} M	1.12	0.94	94.5	2.73	0.92	92.0	5.69	0.89	89.7	12.20	0.86	86.8
64.6×10^{-5} M	0.75	0.96	96.3	2.24	0.93	93.5	4.75	0.91	91.4	10.53	0.88	88.6
MBP												
6.46×10^{-5} M	4.41	0.78	78.2	8.34	0.75	75.8	14.97	0.73	73.0	28.36	0.69	69.4
16.1×10^{-5} M	2.86	0.85	85.8	5.65	0.83	83.6	10.58	0.81	80.9	20.86	0.77	77.5
32.3×10^{-5} M	2.11	0.89	89.6	4.33	0.87	87.4	8.32	0.85	85.0	16.97	0.81	81.7
48.5×10^{-5} M	1.42	0.92	92.9	3.03	0.91	91.2	6.18	0.88	88.8	13.52	0.85	85.4
64.6×10^{-5} M	1.12	0.94	94.4	2.47	0.92	92.8	5.17	0.90	90.7	11.40	0.87	87.7
PMBP												
6.46×10^{-5} M	5.18	0.74	74.3	9.67	0.72	72.0	17.12	0.69	69.1	32.02	0.65	65.4
16.1×10^{-5} M	3.08	0.84	84.7	6.05	0.82	82.5	11.24	0.79	79.7	22.02	0.76	76.2
32.3×10^{-5} M	2.22	0.89	89.0	4.56	0.86	86.8	8.41	0.84	84.1	18.06	0.80	80.5
48.5×10^{-5} M	1.61	0.92	92.0	3.30	0.90	90.4	6.64	0.88	88.0	14.73	0.85	84.1
64.6×10^{-5} M	1.42	0.92	92.9	2.72	0.92	92.1	5.55	0.90	89.9	12.52	0.87	86.5

the compounds was investigated. To the best of our knowledge, the corrosion inhibition properties of the benzimidazole derivatives used in this work have not been reported in any previous work.

2. Experimental

2.1. Synthesis of the benzimidazole derivatives used as corrosion inhibitors

The compounds PzMBP, MBP, and PMBP were synthesized by reported method [21] as shown in Scheme 1. Equimolar mixture of 2-(1*H*-benzimidazol-2-yl)phenol (0.004 mol), formaldehyde (0.004 mol), piperazine or morpholine or piperidine (0.004 mol) and HCl (2 mL) was heated under reflux in methanol for 3 h. The hot mixture was filtered, cooled in ice and the separated solid was filtered and recrystallized with a suitable solvent to give compounds, PzMBP, MBP, and PMBP. The purity of the synthesized compounds was confirmed by thin layer chromatography. The structures of the synthesized inhibitors are shown in Fig. 1. Physico-chemical and spectroscopic data of the synthesized compounds are given below:

2.1.1. PzMBP

MP: 236 °C–238 °C; Elemental analysis (%) calculated/found: C (70.13/70.06); H (6.49/6.64); N (18.18/18.27).

IR (KBr) cm^{-1}: 3285 (—NH, str), 1595 (C═N, str), 3310 (—OH, str), 1255 (—CN, str).

^{1}H NMR (DMSO-*d6*) ppm: 1.26 (s, 2H, CH_2), 9.78 (s, O–H), 7.46 (t, 4H, Ar–H). 2.8 (1s, 1H, N–H), 3.4 (t, 4H, N–CH), 3.6 (t, 4H, NH–CH), 7.22 (m, 4H, Ar).

2.1.2. MBP

MP: 238 °C–240 °C; Elemental analysis (%) calculated/found: C (69.90/69.16); H (6.15/6.24); N (13.59/13.27).

IR (KBr) cm^{-1}: 3245 (—NH, str), 1668 (C═N, str), 3245 (OH, str), 1278 (—CN, str).

^{1}H NMR (DMSO-*d6*) δppm: 1.22 (s, 2H, CH_2), 9.73 (s, O–H), 7.44 (t, 4H, Ar–H), 3.6 (t, 4H, O–CH), 3.8 (t, 4H, N–CH), 7.15 (m, 4H, Ar).

2.1.3. PMBP

MP: 232 °C–234 °C; Elemental analysis (%) calculated/found: C (73.22/72.84); H (7.12/6.94); N (14.24/13.97).

IR (KBr) cm^{-1}: 3330 (—NH, str), 1590 (C═N, str), 3330 (OH, str), 1260 (—CN, str).

^{1}H NMR (DMSO-*d6*) δppm: 1.26 (s, 2H, CH_2), 9.76 (s, O–H), 7.47 (t, 4H, Ar–H), 1.65 (1s, 1H), 2.62 (t, 4H, N–CH), 2.54 (t, 4H), 7.32 (m, 4H, Ar).

2.2. N80 steel sample

Corrosion studies were performed on N80 steel samples having composition (wt.%): C, 0.31; Mn, 0.92; Si, 0.19; S, 0.008; P, 0.010; Cr, 0.20 and Fe balance. N80 steel coupons were cut into the dimension 6.0 cm × 2.5 cm × 0.1 cm and mechanically abraded with different grade emery papers (120, 220, 400, 600, 800, 1500 and 2000 grade) for weight loss experiments. For electrochemical measurements, N80 steel coupons having the dimension 1.0 cm × 1.0 cm × 0.1 cm were mechanically abraded and covered with araldite resin leaving an exposed surface area of 1 cm^2. Prior to the experiments, specimens were washed with distilled water, degreased in acetone, dried and stored in vacuum desiccator.

2.3. Test solution

Analytical reagent grade HCl was diluted with double distilled water to obtain 15% HCl solution. The concentration of inhibitors employed was varied from 6.46×10^{-5} to 64.6×10^{-5} M, and the volume of the electrolyte used was 250 mL for weight loss measurements and 150 mL for electrochemical studies.

2.4. Methods

2.4.1. Weight loss method

Weight loss measurements were performed at different temperatures (303–333 K) by immersing accurately weighed N80 steel test coupons in 250 mL of 15% HCl solution in the absence and presence of different concentrations (6.46×10^{-5} to 64.6×10^{-5} M) of the inhibitors. The immersion time was optimized and the optimized 6 h immersion time was used for all the weight loss measurements. The test

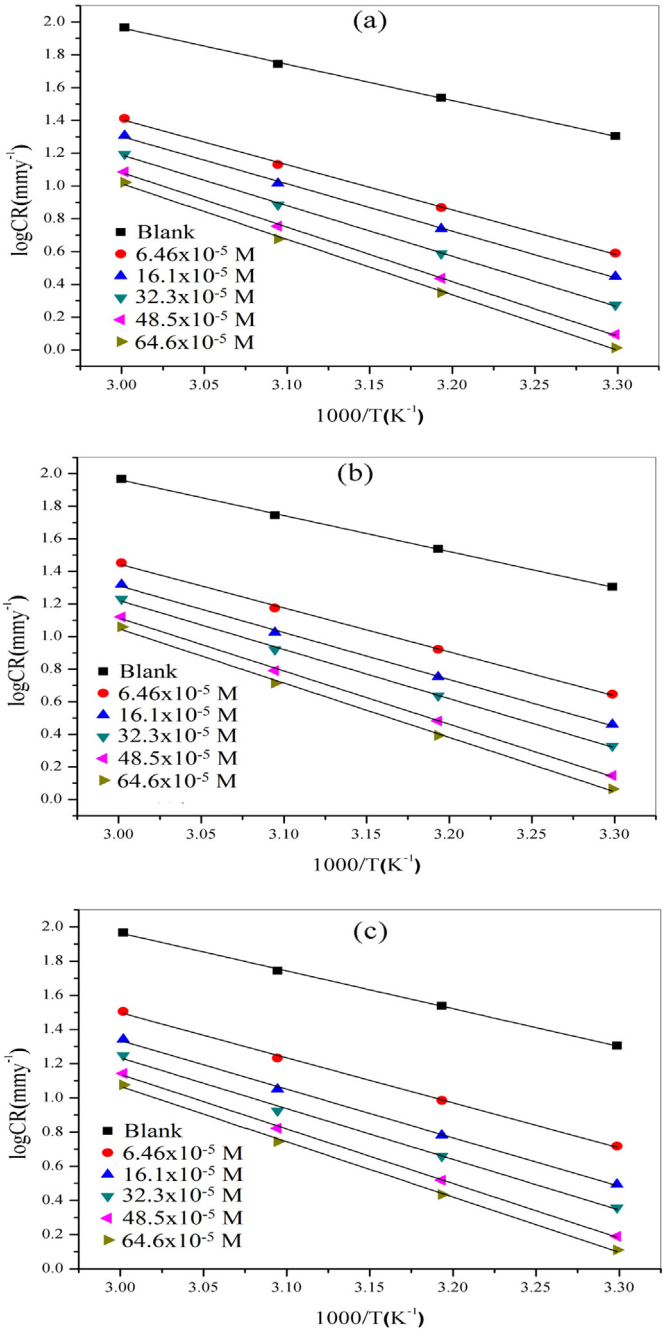

Fig. 2. Arrhenius plots for N80 steel corrosion in 15% HCl solution (a) PzMBP (b) MBP (c) PMBP.

coupons were removed from the electrolyte after 6 h, washed thoroughly with distilled water, dried and weighed. Triplicate experiments were conducted for each concentration of the inhibitors to ensure reproducibility and average weight loss (W) was used to calculate the corrosion rate and inhibition efficiency. The corrosion rate (CR), inhibition efficiency ($\eta\%$) and surface coverage (θ) were determined by following equations [22]:

$$CR(\text{mmy}^{-1}) = \frac{87.6W}{Atd} \quad (1)$$

where, W = average weight loss (mg), A = area of specimen (cm^2) exposed in acidic solution, t = exposure time (h), and d = density of N80 steel ($g\ cm^{-3}$).

$$\theta = \frac{CR_0 - CR_i}{CR_0} \quad (2)$$

$$\eta(\%) = \frac{CR_0 - CR_i}{CR_0} \times 100 \quad (3)$$

where, CR_0 and CR_i are corrosion rates in the absence and presence of inhibitors.

2.4.2. Potentiodynamic polarization studies

Potentiodynamic polarization measurements were carried out in a conventional three-electrode cell consisting of N80 steel working electrode, a platinum counter electrode and a saturated calomel electrode (SCE) as reference electrode. The CH electrochemical workstation (Model No: CHI 760D, manufactured by CH Instruments, Austin, USA) was used and the measurements were taken at 303 K. Before each measurement, the working electrodes were immersed in the test solution until a steady potential was reached. After the establishment of a steady open circuit potential (OCP), potentiodynamic polarization curves were obtained at a scan rate of 0.1 mV s^{-1} in the potential range from −700 to −300 mV vs SCE. Potentiodynamic polarization studies were performed in 15% HCl solution in the absence and presence of various concentrations of the three inhibitors. Corrosion current density (i_{corr}) and corrosion potential (E_{corr}) values were obtained by Tafel extrapolation method. The percentage inhibition efficiency ($\eta\%$), was calculated using the equation:

$$\eta(\%) = \frac{i^0_{corr} - i_{corr}}{i^0_{corr}} \times 100 \quad (4)$$

where i^0_{corr} and i_{corr} are the values of corrosion current density without and with inhibitors, respectively.

2.4.3. Electrochemical impedance spectroscopy (EIS) studies

Impedance measurements were carried out using the same electrochemical cell and workstation as mentioned for polarization measurements in the frequency range from 100 kHz to 10 mHz, using 10 mV peak to peak amplitude ac signal at the OCP. The impedance spectra were recorded as Nyquist and Bode plots. The charge transfer resistance (R_{ct}) was obtained by fitting the impedance spectra with an

Table 2
Activation parameter for N80 steel in 15% HCl solution in the absence and presence of inhibitors obtained from weight loss measurements.

Inhibitor	Concentration (M)	E_a (kJ mol^{-1})	ΔH^* (kJ/mol)	ΔS^* ($Jmol^{-1}\ K^{-1}$)
Blank	–	42.34	39.70	−89.20
PzMBP	6.46×10^{-5} M	52.74	50.10	−68.71
	16.1×10^{-5} M	55.27	52.64	−63.16
	32.3×10^{-5} M	59.09	56.45	−53.78
	48.5×10^{-5} M	63.74	61.10	−41.90
	64.6×10^{-5} M	64.83	62.19	−39.99
MBP	6.46×10^{-5} M	51.65	49.01	−71.20
	16.1×10^{-5} M	55.11	52.47	−63.35
	32.3×10^{-5} M	57.75	55.10	−57.22
	48.5×10^{-5} M	62.50	59.86	−44.97
	64.6×10^{-5} M	63.87	61.23	−42.29
PMBP	6.46×10^{-5} M	50.46	47.82	−73.88
	16.1×10^{-5} M	54.39	51.75	−65.07
	32.3×10^{-5} M	56.78	54.14	−59.90
	48.5×10^{-5} M	61.07	58.43	−48.80
	64.6×10^{-5} M	61.96	59.32	−47.65

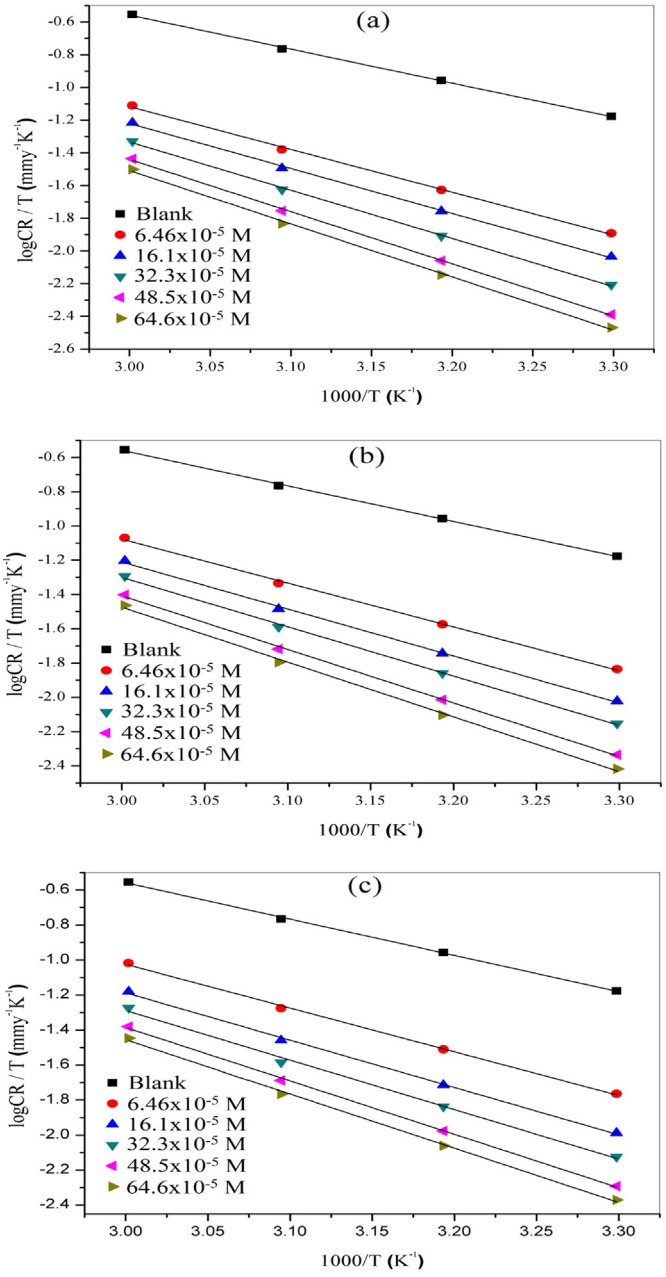

Fig. 3. Transition state plot for N80 steel in 15% HCl solution at different concentrations (a) PzMBP (b) MBP (c) PMBP.

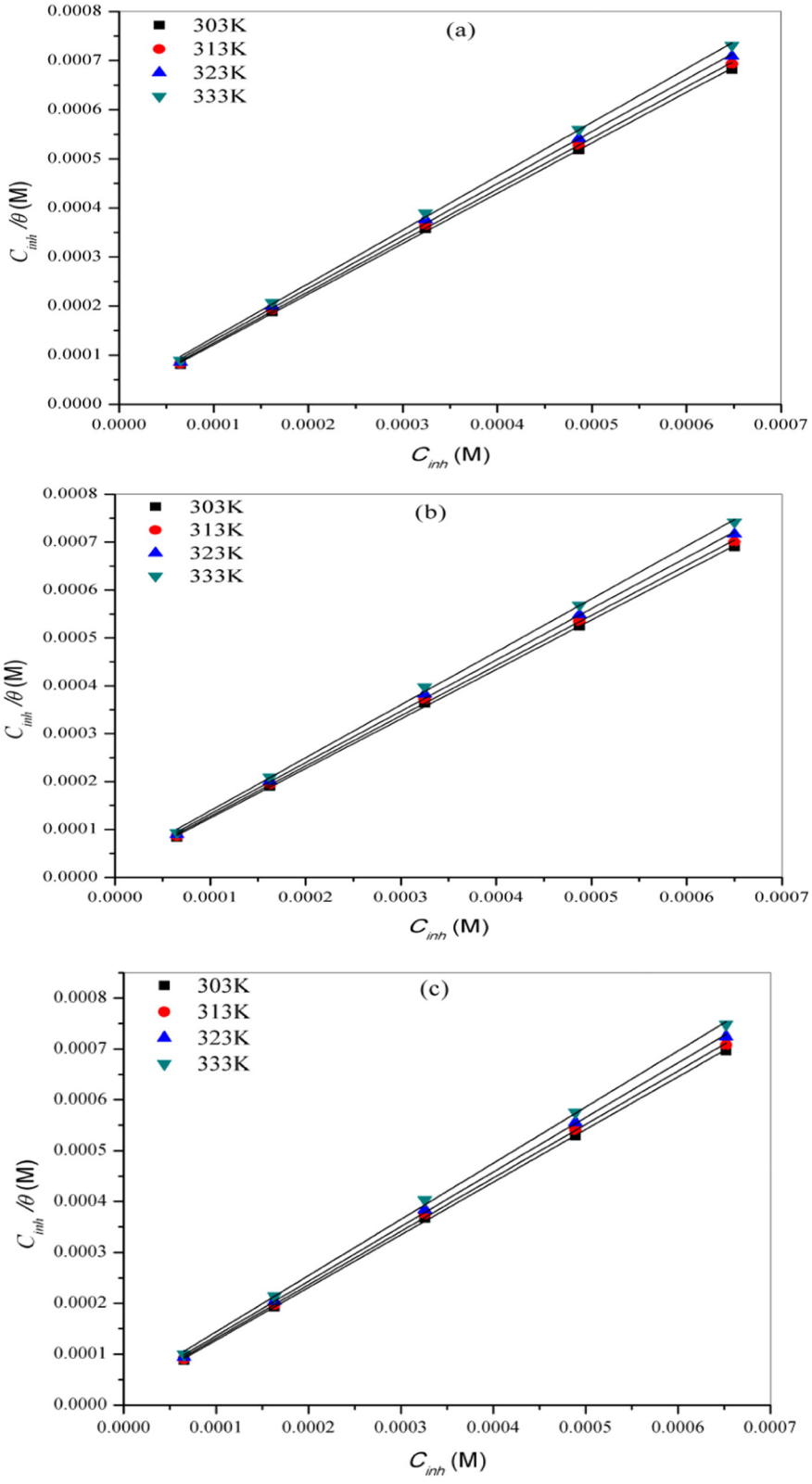

Fig. 4. Langmuir plots for (a) PzMBP (b) MBP (c) PMBP.

appropriate equivalent circuit. The inhibition efficiency ($\eta\%$) was calculated from the R_{ct} values according to the equation:

$$\eta(\%) = \frac{R_{ct\ (inh)} - R_{ct}}{R_{ct\ (inh)}} \times 100 \quad (5)$$

where $R_{ct(inh)}$ and R_{ct} are charge transfer resistances in with and without inhibitor respectively. The values of double layer capacitance (C_{dl}) were calculated from the R_{ct} and CPE parameters (Y_0 and n) using the expression [23]:

$$C_{dl} = \left(Y_0\ {R_{ct}}^{1-n}\right)^{1/n} \quad (6)$$

where Y_0 is CPE constant and n is CPE exponent. The value of n represents the deviation from the ideal behavior and it lies between 0 and 1.

2.4.4. UV–visible spectra

The UV–visible absorption spectra of the inhibitor solutions before and after 6 h of N80 steel immersion were recorded using the Shimadzu model UV-160A spectrophotometer.

2.4.5. FTIR spectrum analysis

The FTIR spectrum of the pure compound and the film formed on the surface of N80 steel specimens was recorded on Perkin Elmer FTIR (Spectrum—2000) spectrophotometer.

2.4.6. Scanning electron microscopy analyses

The N80 steel specimens of size 1.0 cm × 1.0 cm × 0.1 cm were abraded with a series of emery paper (grade 320–500–800–1200) and then washed with distilled water and acetone. After immersion in 15% HCl solution in the absence and presence of 64.6×10^{-5} M concentration of the inhibitors, PzMBP, MBP and PMBP at 303 K for 6 h, the specimens were cleaned with distilled water, dried with a cold air blaster, and then the SEM images were recorded using a Traktor TN-2000 energy dispersive spectrometer and JEOL JSM-6380 LA analytical scanning electron microscope in the vacuum mode by instrument operated at 10 kV.

2.4.7. Atomic force microscopy

The morphology of the N80 steel surface in 15% HCl without and with 64.6×10^{-5} M of the studied inhibitors was investigated by atomic force microscopy (AFM). For AFM analysis the N80 steel specimens of size 1 cm × 1 cm × 0.1 cm were immersed in the test solution in the absence and presence of inhibitors for 6 h at room temperature. Then the specimens were taken out from the solution, cleaned with distilled water, dried and used for the AFM analyses. The AFM analyses were carried out using a Nanosurf Easyscan 2 instrument.

2.4.8. Quantum chemical study

Complete geometrical optimization of the investigated inhibitors was performed using Density Functional Theory (DFT) in the aqueous phase (protonated form) with the Becke's three parameter exchange functional along with the Lee–Yang–Parr nonlocal correlation functional (B3LYP) with 6-31G (d, p) basis set implemented in Gaussian 03 program package [24,25]. Quantum chemical parameters such as the energies of the highest occupied and lowest unoccupied molecular orbitals (E_{HOMO} and E_{LUMO} respectively), energy gap (ΔE), dipole moment (μ), global hardness (η) and softness (σ) and fraction of electrons transferred from the inhibitor molecule to the metal surface (ΔN) were calculated. Mulliken charges on *HOMO* and *LUMO* orbitals were also obtained for the molecules.

3. Results and discussion

3.1. Weight loss measurements

Corrosion of N80 steel in 15% HCl solution in the absence and presence of different concentrations of the inhibitors (PzMBP, MBP and PMBP) at different temperatures (303–333 K) was monitored using weight loss method.

3.1.1. Effect of inhibitor concentration

The corrosion inhibition efficiencies (η%) of the inhibitors PzMBP, MBP and PMBP after 6 h of immersion at 303 K as evaluated by the weight loss technique are listed in Table 1. It is apparent from Table 1 that inhibition efficiency increases with increase in concentration of the inhibitors. It is further evident from Table 1 that all the three inhibitors show appreciably high η% even at the concentration as low as 6.46×10^{-5} M. The of PzMBP, MBP and PMBP was found to be 96.3, 94.4 and 92.9% respectively at 64.6×10^{-5} M, and 80.7, 78.2 and 74.3% respectively at 6.46×10^{-5} M and 303 K (Table 1). The η% of PzMBP, MBP and PMBP over the range of concentration studied is higher than what have been reported for some imidazole derivatives in literature [15–19]. The increase in η% with increasing concentration of inhibitors was due to increase in the surface coverage, which results in enhanced retardation of metal dissolution in the aggressive media [26,27]. PzMBP with four N-atoms in its molecules showed better inhibition performance than MBP and PMBP with three N-atoms each. This further supports previous reports that the presence of heteroatoms in an organic molecule facilitates adsorption onto metal surface and enhances corrosion inhibition [9–13].

Table 3
Adsorption parameters for PzMBP, MBP and PMBP calculated from Langmuir adsorption isotherm for N80 steel in 15% HCl solution at 303–333 K.

Inhibitor	Temperature (K)	K_{ads} (M^{-1})	ΔG°_{ads} (kJ mol^{-1})	Slope	R^2
PzMBP	303 K	5.29×10^4	−37.54	0.99	0.999
	313 K	4.80×10^4	−38.53	0.98	0.995
	323 K	4.20×10^4	−39.38	1.01	0.986
	333 K	3.74×10^4	−40.27	1.02	0.985
MBP	303 K	4.87×10^4	−37.34	0.97	0.994
	313 K	4.34×10^4	−38.26	0.99	0.993
	323 K	3.90×10^4	−39.19	0.98	0.994
	333 K	3.48×10^4	−40.09	1.01	0.989
PMBP	303 K	4.19×10^4	−36.69	0.99	0.988
	313 K	3.83×10^4	−37.66	1.03	0.995
	323 K	3.49×10^4	−38.62	1.02	0.994
	333 K	2.98×10^4	−39.38	0.99	0.997

3.1.2. Effect of temperature

Effect of temperature on the corrosion of N80 steel in 15% HCl without and with various concentrations of the studied inhibitors was investigated between 303 K and 333 K. Corrosion parameters such as corrosion rate (*CR*), surface coverage (θ) and η% obtained from weight loss measurements at various concentrations and temperatures are shown in Table 1. It is clear from the Table 1 that the corrosion rate increases with increase in temperature in the presence and absence of the inhibitors. The corrosion rate of N80 steel in the absence of inhibitors increased steeply from 303 to 333 K whereas the corrosion rate increases slowly in the presence of inhibitors. The η% decreased with increasing temperature from 303 to 333 K. This type of behavior can be described

Table 4
Potentiodynamic polarization parameters for corrosion of N80 steel in 15% HCl solution in the presence or absence of different concentrations of inhibitors at 303 K.

Concentration (M)	E_{corr} (mV vs SCE)	β_a (mV dec^{-1})	β_c (mV dec^{-1})	i_{corr} (μA cm^{-2})	η%
Blank	−495	93	142	568	–
PzMBP					
6.46×10^{-5} M	−496	83	146	107.6	81.05
16.1×10^{-5} M	−494	98	151	73.8	87.00
32.3×10^{-5} M	−503	105	134	52.1	90.82
48.5×10^{-5} M	−505	101	141	34.6	93.91
64.6×10^{-5} M	−508	91	155	28.4	95.00
MBP					
6.46×10^{-5} M	−492	92	131	113	80.1
16.1×10^{-5} M	−495	96	133	86	84.9
32.3×10^{-5} M	−496	88	130	62	89.1
48.5×10^{-5} M	−498	78	127	41	92.8
64.6×10^{-5} M	−502	87	102	38	93.3
PMBP					
6.46×10^{-5} M	−488	78	122	148	73.4
16.1×10^{-5} M	−497	84	152	102	82.1
32.3×10^{-5} M	−497	92	130	66	88.3
48.5×10^{-5} M	−501	110	125	52	90.8
64.6×10^{-5} M	−502	105	14	48	91.5

on the basis that increase in temperature leads to a shift of the equilibrium position of the adsorption/desorption phenomenon towards desorption of the inhibitors molecules at the surface of N80 steel [28].

3.1.3. Thermodynamic and activation parameters

The apparent activation energy (E_a) for dissolution of N80 steel in 15% HCl solution without and with various concentrations of the inhibitors was calculated by using the Arrhenius equation (7):

$$\log CR = \frac{-E_a}{2.303\,RT} + \log A \tag{7}$$

where E_a is the apparent activation energy, R is the molar gas constant (8.314 J K^{-1} mol^{-1}), T is the absolute temperature (K) and A is the Arrhenius pre-exponential factor. The Arrhenius plots of log CR against $1/T$ for the corrosion of N80 steel in 15% HCl solution in the absence and presence of various concentrations of PzMBP, MBP and PMBP are shown in Fig. 2. The slopes of the lines were determined and the respective values of E_a were calculated from the slopes ($E_a = -\text{slope} \times 2.303R$). The calculated values of E_a are listed in Table 2. It is evident from the values of E_a in Table 2 that the values of the E_a for the inhibitors-containing systems were higher than that for the uninhibited system, indicating a decrease in the rate of dissolution of N80 steel in the acid due to an increase in energy barrier for the dissolution reaction, which in turn is associated with the adsorption of the inhibitors on the metal surface [29,30].

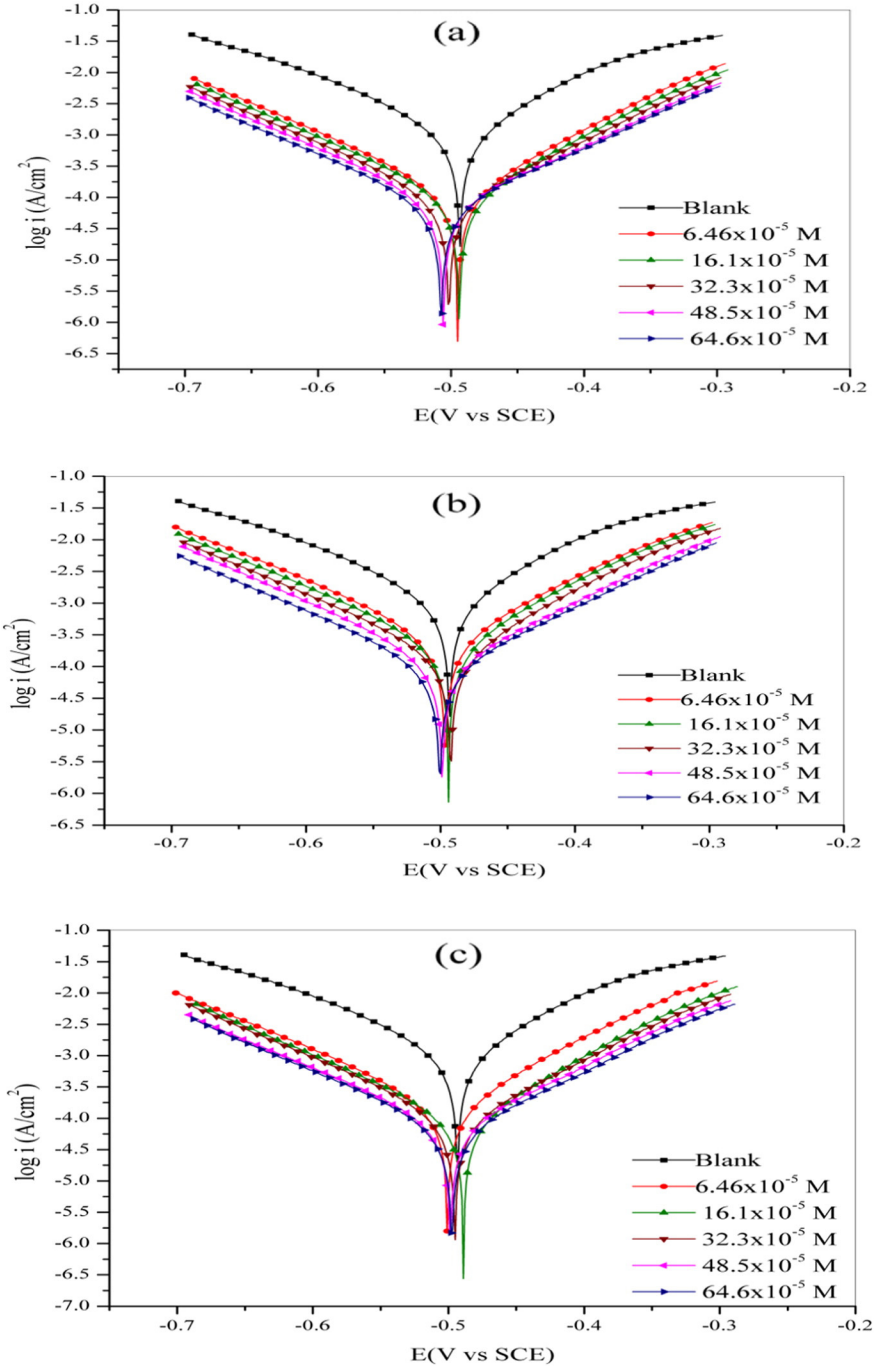

Fig. 5. Potentiodynamic polarization curves for N80 steel in 15% HCl solution in the presence and absence of inhibitor 303 K. (a) PzMBP (b) MBP (c) PMBP.

The values of standard enthalpy of activation (ΔH^*) and standard entropy of activation (ΔS^*) were calculated by using the equation:

$$CR = \frac{RT}{Nh}\exp\left(\frac{\Delta S^*}{R}\right)\exp\left(-\frac{\Delta H^*}{RT}\right) \quad (8)$$

where, h is Planck's constant and N is the Avogadro number.

A plot of log (CR/T) against $1/T$ (Fig. 3) gave straight lines with a slope of $-\Delta H^*/2.303R$ and an intercept of $[\log(R/Nh) + (\Delta S^*/2.303R)]$ from which the value of activation thermodynamic parameters ΔH^* and ΔS^* were calculated and listed in Table 2. The positive sign of the ΔH^* implies that the dissolution of N80 steel is endothermic. The negative value of ΔS^* for all the three the inhibitors indicates that the

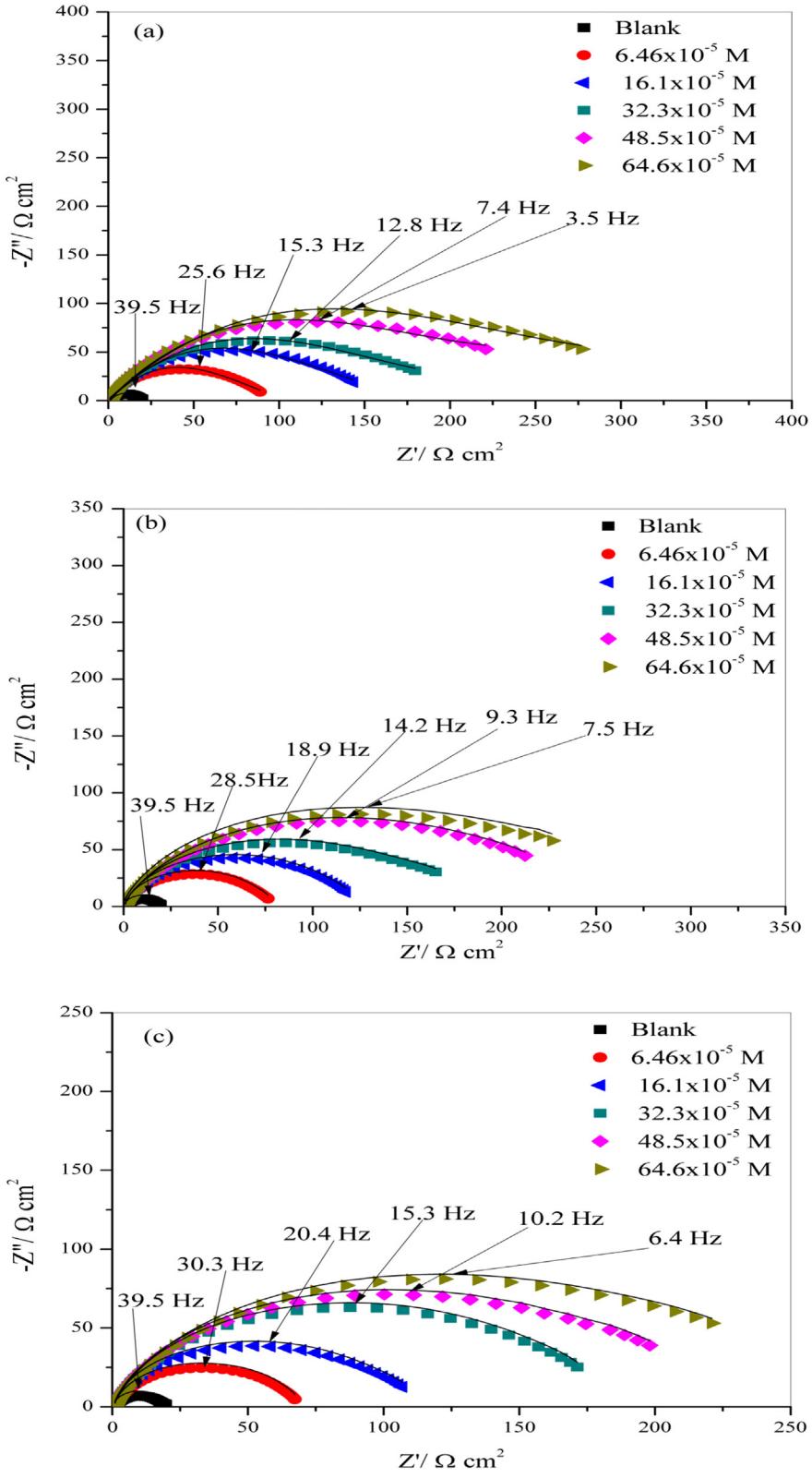

Fig. 6. Experimental (symbols) and fitting (solid lines) Nyquist plots for N80 steel in 15% HCl solution containing various concentrations of (a) PzMBP (b) MBP (c) PMBP. at 303 K.

formation of the activated complex in the rate determining step represents an association rather than a dissociation step, meaning that a decrease in disorderliness takes place during the course of the transition from reactants to activated complex [31].

3.2. Adsorption isotherm

Basic information on the interaction between the organic inhibitors and the N80 steel surface are obtained from various adsorption isotherms. The most commonly used adsorption isotherms are Langmuir, Temkin, and Frumkin isotherms. The experimental data were fitted into various adsorption isotherms but Langmuir isotherm gave the best linear plots. The plots of C_{inh}/θ vs C_{inh} at different temperatures yielded straight lines as shown in Fig. 4. The slope and the correlation coefficient (R^2) values for the Langmuir adsorption plots are listed in Table 4. The correlation coefficient and slope values in Table 4 are near to unity, indicating that the adsorption of these inhibitors on N80 steel surface obey Langmuir adsorption isotherm represented by the equation:

$$\frac{C_{inh}}{\theta} = \frac{1}{K_{ads}} + C_{inh} \tag{9}$$

where, C_{inh} is the inhibitor concentration, K_{ads} is the equilibrium constant for adsorption–desorption process. From the intercepts of Fig. 4, the values of K_{ads} were calculated. Large values of K_{ads} obtained for all the three studied inhibitors imply more efficient adsorption and hence better corrosion inhibition efficiency. Using the values of $K_{ads,}$ the values of ΔG°_{ads} were evaluated by using the equation:

$$\Delta G^{0}_{ads} = -RT \ln(55.5 K_{ads}) \tag{10}$$

where R is the gas constant and T is the absolute temperature (K). The value of 55.5 is the concentration of water in solution in mol L^{-1}. The calculated values of K_{ads} and ΔG°_{ads} are listed in Table 3. In general, the values of ΔG°_{ads} up to -20 kJ mol^{-1} are associated with the electrostatic interaction between charged inhibitor molecules and charged metal surface (physisorption) and those which are more negative than -40 kJ mol^{-1} involve charge sharing or charge transfer from the inhibitor molecules to the metal surface [32] (chemisorption). The calculated ΔG°_{ads} values for PzMBP, MBP and PMBP were found in the range of -37.54 to -40.27, -37.34 to -40.09 and -36.69 to -39.38 kJ mol^{-1} respectively at different temperatures (303–333 K). These values are between the threshold values for physical and chemical adsorption mechanisms indicating that the adsorptions of PzMBP, MBP and PMBP on N80 steel surface involve competitive physisorption and chemisorption mechanisms. Quraishi and Shukla [33] studied 4-substituted anilinomethylpropionate as corrosion inhibitors for mild steel in hydrochloric acid solution. The Gibbs free energy of adsorption for these molecules were reported to be around -38 kJ mol^{-1} and it was concluded that the adsorption mechanism of these molecules on steel involved both chemisorption and physisorption interactions. Similar conclusion was also reported by Ozcan [34], who studied the inhibition effect of cystine on mild steel corrosion in sulfuric acid. Thus, the calculated values of ΔG°_{ads} (Table 4) for all the three inhibitors suggest that the adsorption of these inhibitors on the surface of N80 steel is not simple physisorption or chemisorption but rather a combination of both mechanisms.

3.3. Electrochemical studies

3.3.1. Polarization studies

The potentiodynamic polarization curves for N80 steel in 15% HCl solution in the absence and presence of various concentrations of PzMBP, MBP and PMBP at 303 K are shown in Fig. 5. It is apparent from Fig. 5 that the nature of the polarization curves remains the same in the absence and presence of the inhibitors but the curves shifted towards lower current density in the presence of inhibitors indicating that the inhibitor molecules retard the corrosion process without altering the mechanism of corrosion. The electrochemical parameters such as corrosion potential (E_{corr}), anodic Tafel slope (β_a), cathodic Tafel slope (β_c) and corrosion current density (i_{corr}) were obtained by extrapolating the anodic and cathodic Tafel regions of the curves to the point of intersection with the E_{corr}. The $\eta\%$ was calculated according to Eq. 4 and the results are given in Table 4. The results in Table 4 revealed that increasing concentration of all the three inhibitors resulted in decrease in i_{corr} and increase in $\eta\%$, which suggests that the inhibitors adsorbed on N80 steel surface to form protective film thereby reducing the exposed active sites on the steel surface [35]. The $\eta\%$ values of the inhibitors are in the order: PzMBP > MBP > PMBP at 303 K, which is in agreement with the trend observed from the weight loss experiments. The presence of inhibitors caused minor change in E_{corr} values with respect to the E_{corr} in the absence of inhibitors. This implies that the inhibitors act as mixed type inhibitors, retarding the rate of both anodic and cathodic reactions [36]. If the displacement in E_{corr} is more than ± 85 mV relating to corrosion potential of the blank, the inhibitor can be considered as a cathodic or anodic type [37]. If the change in E_{corr} is less than ± 85 mV, the corrosion inhibitor may be regarded as a mixed type. The maximum displacement in E_{corr} in the present study is 13 mV, which indicates that PzMBP, MBP and PMBP are mixed type inhibitor.

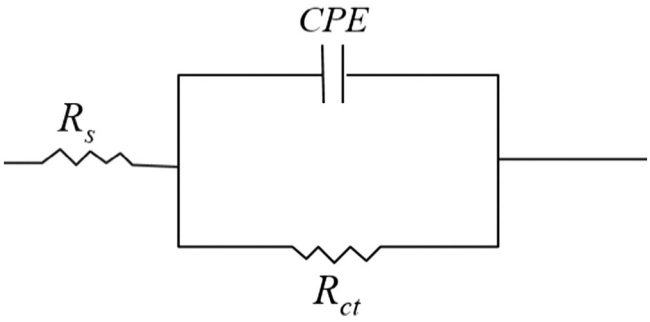

Fig. 7. Equivalent circuit applied for fitting of the impedance spectra.

Table 5
EIS parameters for corrosion of N80 steel in 15% HCl solution in the presence or absence of different concentrations of inhibitors at 303 K.

Concentration (M)	R_s (Ω cm^2)	R_{ct} (Ω cm^2)	Y_0 (μF cm^{-2})	n	C_{dl} (μF cm^{-2})	$\eta\%$
BLANK	0.64	25	695	0.80	252	–
PzMBP						
6.46×10^{-5} M	0.75	119	163.0	0.84	75.3	78.9
16.1×10^{-5} M	0.78	178	100.2	0.87	54.4	86.0
32.3×10^{-5} M	0.88	228	65.73	0.90	41.2	89.1
48.5×10^{-5} M	0.74	308	44.37	0.93	32.1	91.9
64.6×10^{-5} M	0.76	364	28.61	0.96	23.8	93.1
MBP						
6.46×10^{-5} M	0.84	104	205.7	0.83	89.2	76.0
16.1×10^{-5} M	0.85	156	131.3	0.86	67.8	83.9
32.3×10^{-5} M	0.80	210	58.31	0.89	48.3	88.1
48.5×10^{-5} M	0.76	278	49.52	0.92	34.2	91.0
64.6×10^{-5} M	0.75	318	36.01	0.95	28.3	92.1
PMBP						
6.46×10^{-5} M	0.63	89	250.2	0.82	102.8	71.9
16.1×10^{-5} M	0.85	147	151.3	0.85	74.7	82.9
32.3×10^{-5} M	0.72	208	117.6	0.88	50.3	87.9
48.5×10^{-5} M	0.61	272	58.2	0.91	38.2	90.9
64.6×10^{-5} M	0.26	300	46.8	0.94	35.4	91.7

3.3.2. EIS studies

The Nyquist plots obtained for N80 steel in 15% HCl solution without and with the various concentrations of PzMBP, MBP and PMBP at 303 K are shown in Fig. 6. The Nyquist plots in Fig. 6 show single semicircles with centers below the real impedance axis for all three inhibitors, indicating that the dissolution of N80 steel in the studied electrolyte systems is controlled by single charge transfer process. The Nyquist plots in the absence and presence of inhibitors are characterized by one capacitive loop. The capacitive loops are not perfect semicircles because of non-homogeneity and roughness of the N80 steel surface [38].

The EIS spectra were analyzed using the equivalent circuit of the form shown in Fig. 7, which comprises parallel combination of the charge transfer resistance (R_{ct}) and the constant phase element (CPE), both in series with the solution resistance (R_s). This type of electrochemical equivalent circuit was reported previously to model the iron/acid interface [39]. Constant phase element (CPE) is introduced instead of pure double layer capacitance to give more accurate fit as the double layer at interface does not behave as ideal capacitor.

The electrochemical parameters obtained from the fitting of the impedance spectra are presented in Table 5. The data shown in Table 5 reveal that the R_{ct} values in the presence of inhibitors are larger than the R_{ct} for the blank. The increase in R_{ct} values is attributed to the formation of insulating protective film of the inhibitors at the metal/solution interface. The CPE value decreases on increasing the concentration of all the

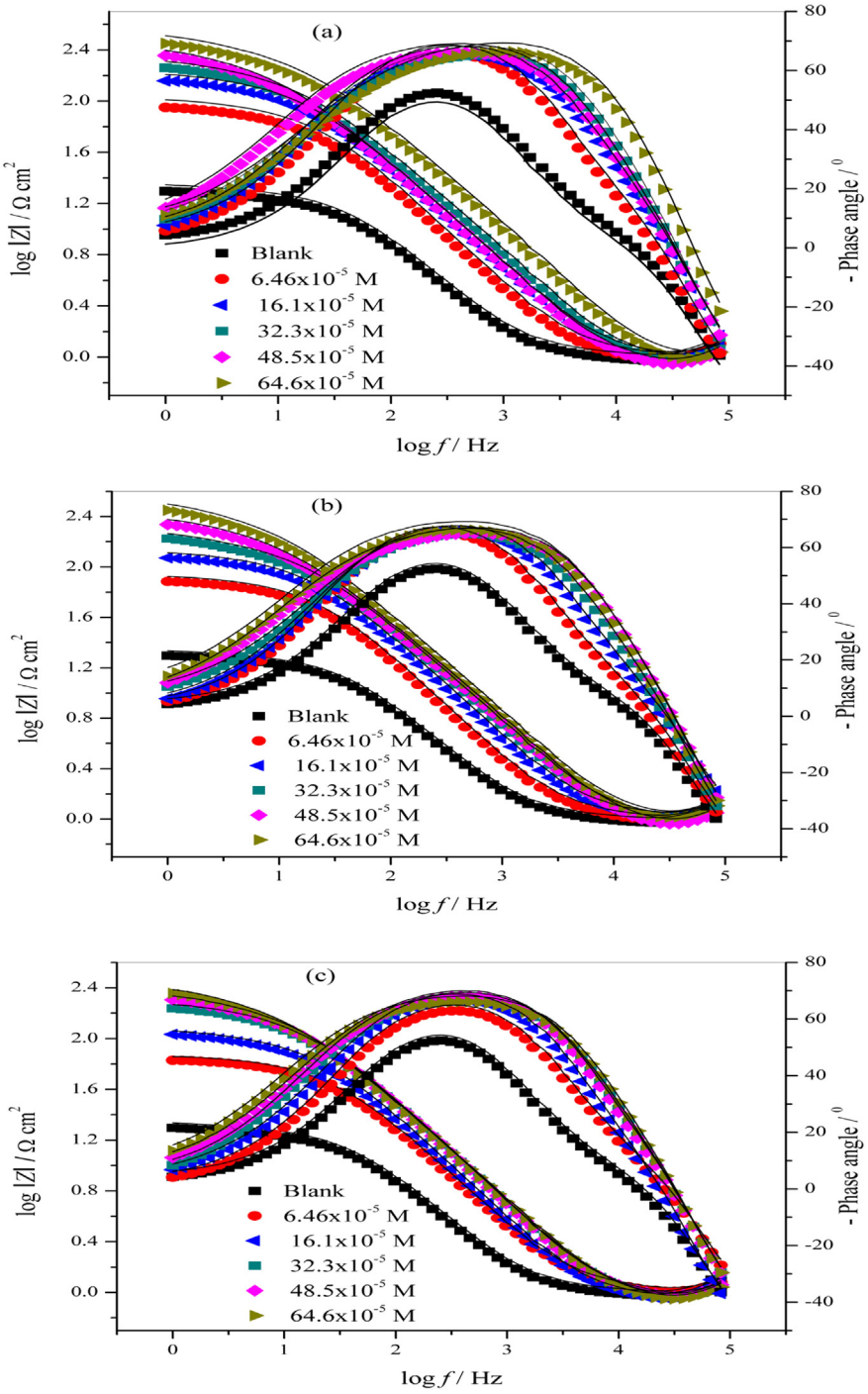

Fig. 8. Experimental (symbols) and fitting (solid lines) Bode plots for N80 steel in 15% HCl solution in the absence and presence of different concentrations of inhibitors (a) PzMBP (b) MBP (c) PMBP.

three inhibitors, indicating the adsorption of the inhibitor molecules on surface of N80 steel.

The impedance Bode plots for N80 steel in 15% HCl solution without and with the various concentrations of PzMBP, MBP and PMBP at 303 K are shown in Fig. 8. The single peak obtained in Bode plots for all the three inhibitors implies that the simple one-time constant equivalent Randle's circuit model used in fitting the impedance spectra was appropriate. The Bode plots show only one phase maximum for all the three inhibitors, indicating that the electrochemical system involves only one relaxation process, which is the charge transfer process taking place at the metal–electrolyte interface. As shown in Fig. 8, the impedance values in the presence of inhibitors are larger than in the absence of inhibitors and increase with increasing concentration of the studied inhibitors. The $\eta\%$ values were calculated according to Eq. 5 and are listed in Table 5. The results are in good agreement with those obtained from weight loss and polarization experiments.

The minor differences in the results from weight loss and electrochemical experiments are not unexpected and have been attributed to the fact that weight loss measurement determines corrosion rate chemically, independent of the electrode potential, whereas electrochemical measurements depend on operational potential [40].

3.4. UV–visible spectroscopy

UV–visible spectroscopy provides a strong evidence for the formation of a metal complex. The UV–visible absorption spectra for 64.6×10^{-5} M solution of inhibitors at 308 K before and after 6 h of N80 steel immersion were obtained and the profiles are shown in

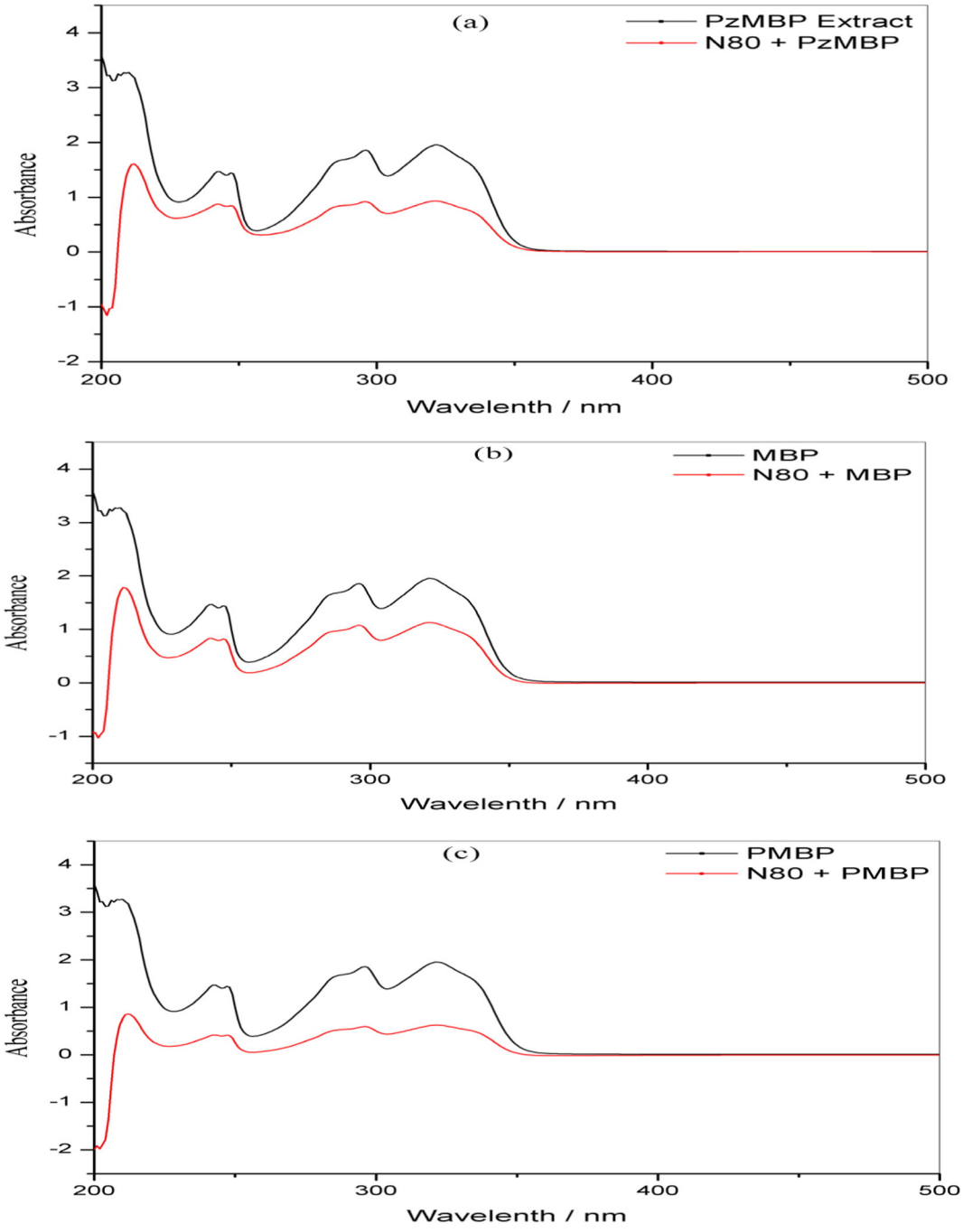

Fig. 9. UV–visible absorption spectra of various solutions before and after immersion of the N80 steel specimen for 6 h in the presence of inhibitors.

Fig. 9. The electronic absorption spectrum of the inhibitors before the N80 steel immersion shows bands in UV–visible region due to π–π* and n–π* transitions with a considerable charge transfer character. After 6 h immersion of N80 steel in the inhibitors, the observed change in the position of absorption maximum and/or change in absorbance values indicate the interaction between Fe^{2+} and inhibitors in 1 M HCl solution.

3.5. Analysis of FTIR spectra

The FTIR spectra of pure inhibitors and reflectance absorption FTIR spectra of the N80 steel retrieved from the solutions of the inhibitors after 6 h immersion time were recorded and represented in Fig. 10. The pure compounds show the IR bands around 3330, 1600 and 1265 cm^{-1} due to the presence of —OH, —NH, C═N and C–N respectively. FTIR spectra of the exposed specimen in the inhibitors show bands around 3390, 1630 and 1165 cm^{-1} due to the presence of —OH, —NH, C═N and C–N respectively. The shifts in vibrational frequency of these groups with respect to pure compound indicate the adsorption of inhibitors through these groups on the N80 steel surface. The presence of the other bands of the inhibitor with minor shift in reflectance spectra of the exposed specimen was also reported which indicates the interaction of the inhibitor molecule with the N80 steel.

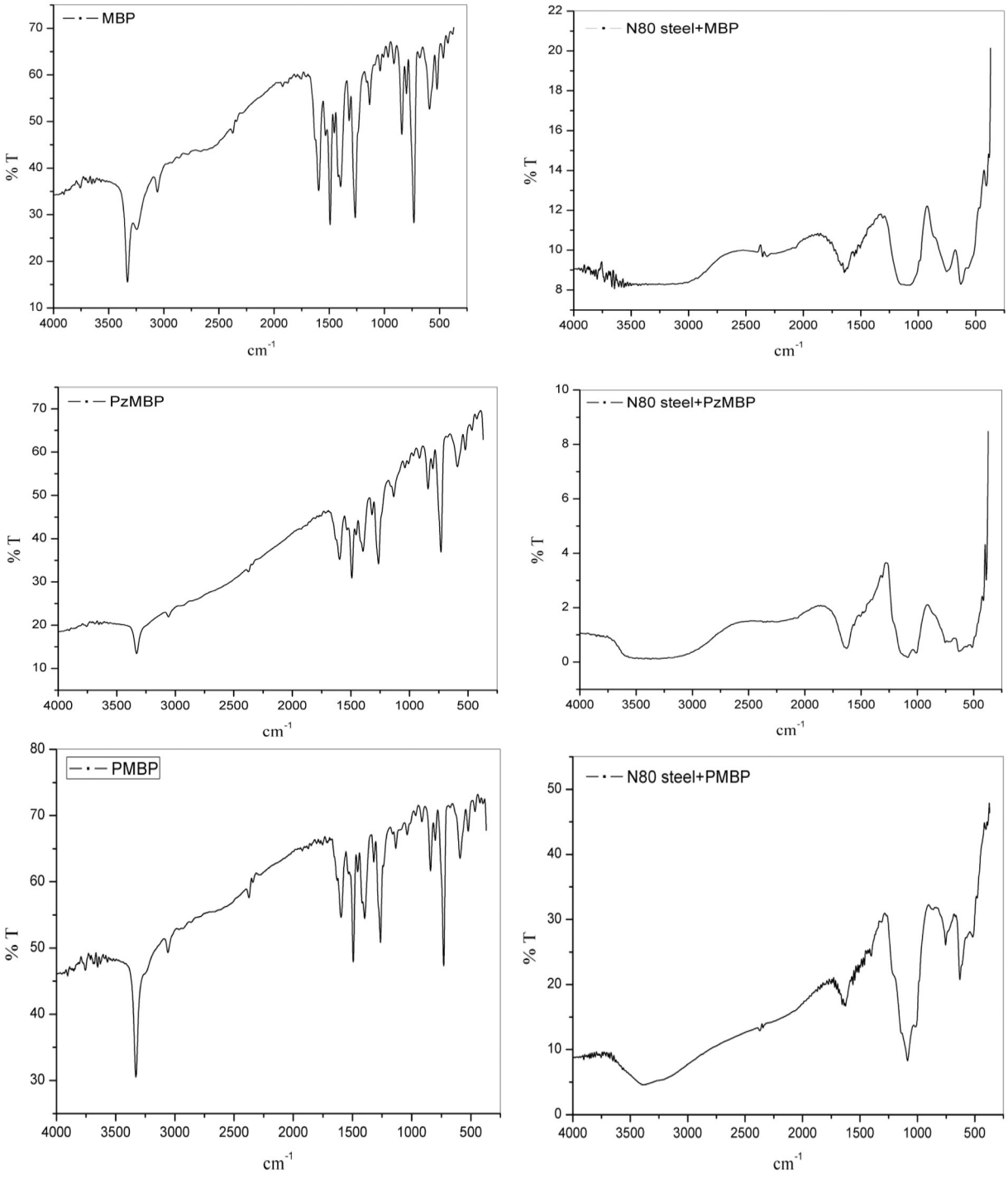

Fig. 10. FTIR spectrum of the pure inhibitors and film formed on the surface of N80 steel specimen.

3.6. Scanning electron microscopy

The surface morphology of the N80 steel samples in 15% HCl solution in the absence and presence of 64.6×10^{-5} M of PzMBP, MBP and PMBP are shown in Fig. 11. Fig. 11a is the SEM of the freshly polished N80 steel sample before immersion in 15% HCl solution. The badly damaged surface (Fig. 11b) obtained when the metal was kept in 15% HCl solution for 6 h without the inhibitors indicates direct acid attack on the metal and high corrosion rate. However, in the presence of the inhibitors, the surfaces of the N80 steel specimens were not as damaged or corroded as in the absence of the inhibitors. The relatively smooth surface observed in the presence of the inhibitors is due to the formation of protective film of the inhibitor on N80 steel surface which shields the surface against direct acid attack.

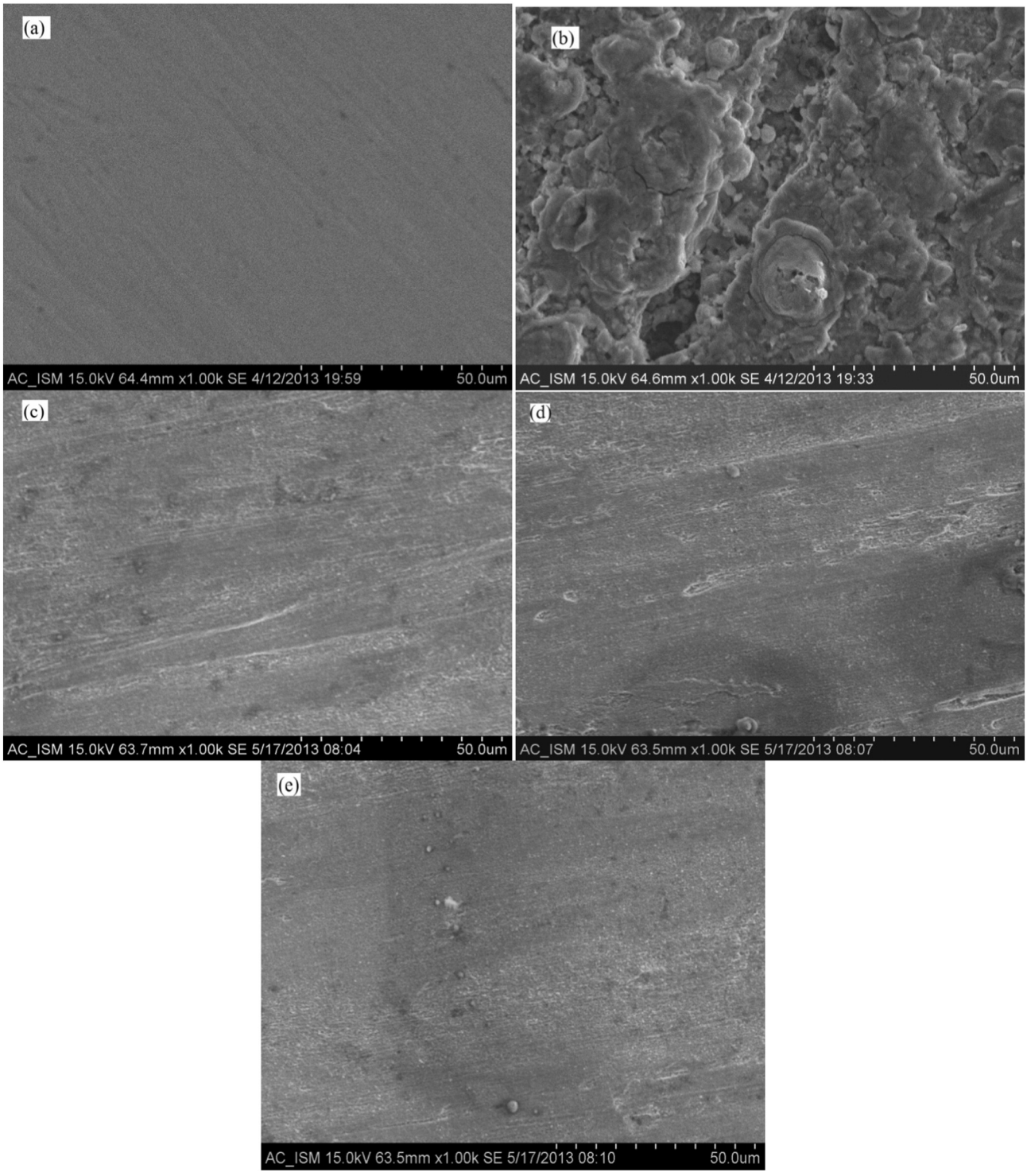

Fig. 11. SEM image of N80 steel in 15% HCl solution after 6 h immersion at 303 K (a) before immersion (polished) (b) after immersion without inhibitor (c) in the presence of inhibitor PzMBP (d) in the presence of inhibitor MBP (e) in the presence of inhibitor PMBP.

3.7. Atomic force microscopy

Surface morphology of the polished N80 steel and N80 steel in 15% HCl solution in the absence and presence of 64.6×10^{-5} M of the inhibitors were investigated through atomic force microscopy (AFM). The results are shown in Fig. 12. The average roughness parameters of polished N80 steel (Fig. 12a) and N80 steel in 15% HCl solution without inhibitor (Fig. 12 b) were found as 25 and 650 nm. There is clear observation of cracks on the steel surface in Fig. 12(b) due to acid attack on the N80 steel surface. However in the presence of 200 ppm of PzMBP, MBP and PMBP, (Figs. 12 (c), (d) and (e) respectively) the average roughness parameters reduced to 70, 85 and 92 nm, respectively. The lowest value of the calculated roughness parameter for PzMBP reveals that PzMBP protects the N80 steel surface more efficiently than MBP and PMBP in 15% HCl solution.

3.8. Quantum chemical calculations

In order to study the effect of molecular structure or reactivity of the studied compounds on their inhibition efficiency, quantum chemical calculations were performed in aqueous phase by using DFT method. The optimized structures, *HOMO* and *LUMO* electron density surfaces of the studied molecules are shown in Fig. 13. For all the three benzimidazole derivatives, the HOMO and LUMO orbitals are π-type orbitals and the electron densities are essentially delocalized over the benzimidazole ring and the adjacent phenolic ring attached to the C2 atom of the benzimidazole. These indicate the reactive sites of the inhibitors for interaction between inhibitor molecules and N80 steel surface. The saturated ring attached to the N1 atom of benzimidazole does not make any significant contribution to the HOMO and LUMO of all the three molecules. The graphical surfaces of the Mulliken electron charge density of the optimized structures of the inhibitors are shown in Fig. 14. A combination of Mulliken population analysis and *HOMO* electron density distribution has been reported to provide good information about possible adsorption centers of the inhibitor molecules [41–43]. The general interpretation given by several authors is that the higher is the magnitude and the number of negatively charged heteroatom present in an inhibitor molecule, the higher the ability to be adsorbed on the metal surface via donor–acceptor mechanism [42] and the more negatively charged regions with major distribution of the *HOMO* are also interpreted as possible centers of adsorption. Mulliken charges according to the numeration of corresponding atoms are shown in Fig. 14. It is evident

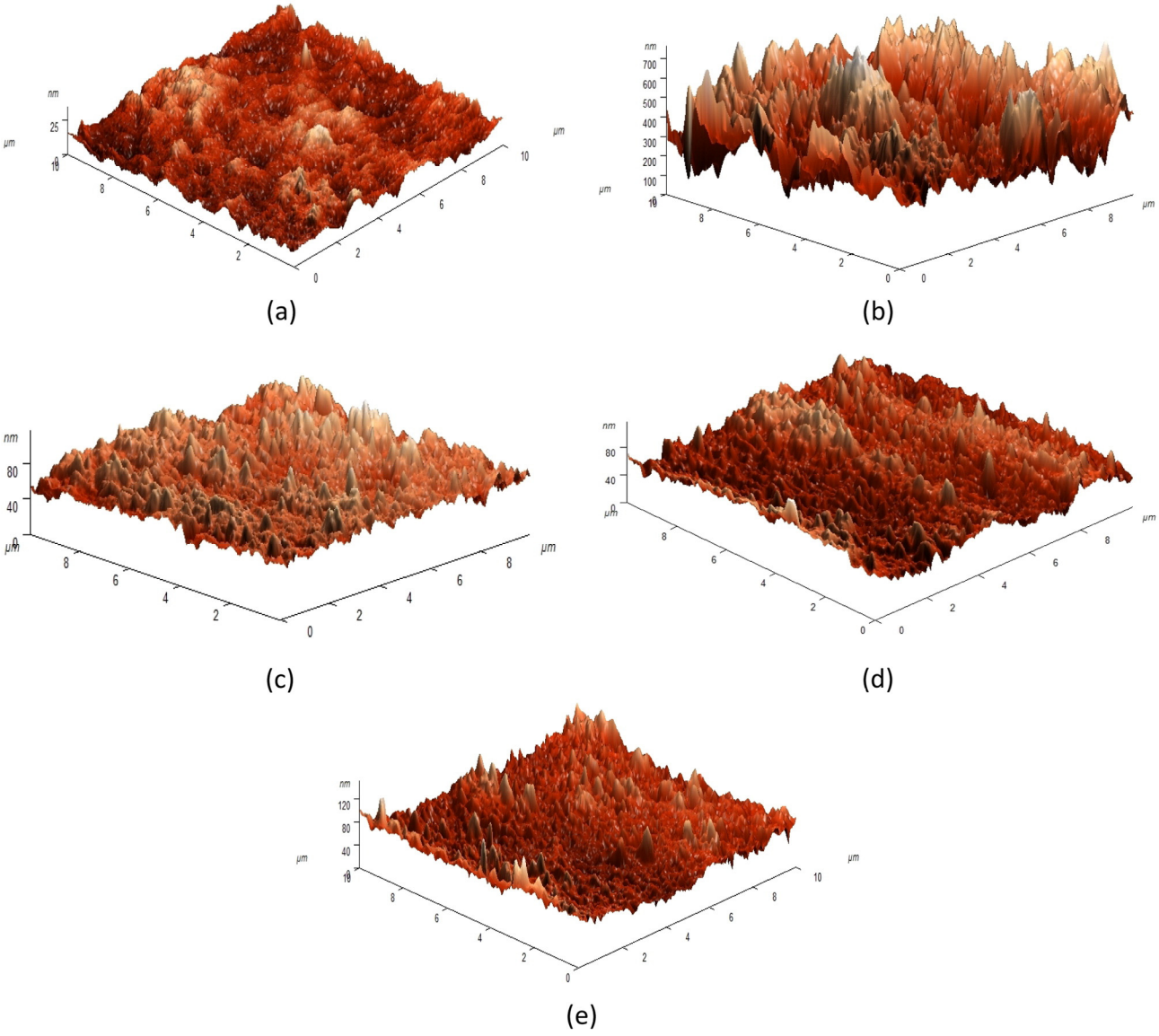

Fig. 12. AFM micrograph of mild steel surface (a) polished mild steel (b) blank in 15% HCl solution (c) with 64.6×10^{-5} M PzMBP (d) with 64.6×10^{-5} M MBP (e) with 64.6×10^{-5} M PMBP.

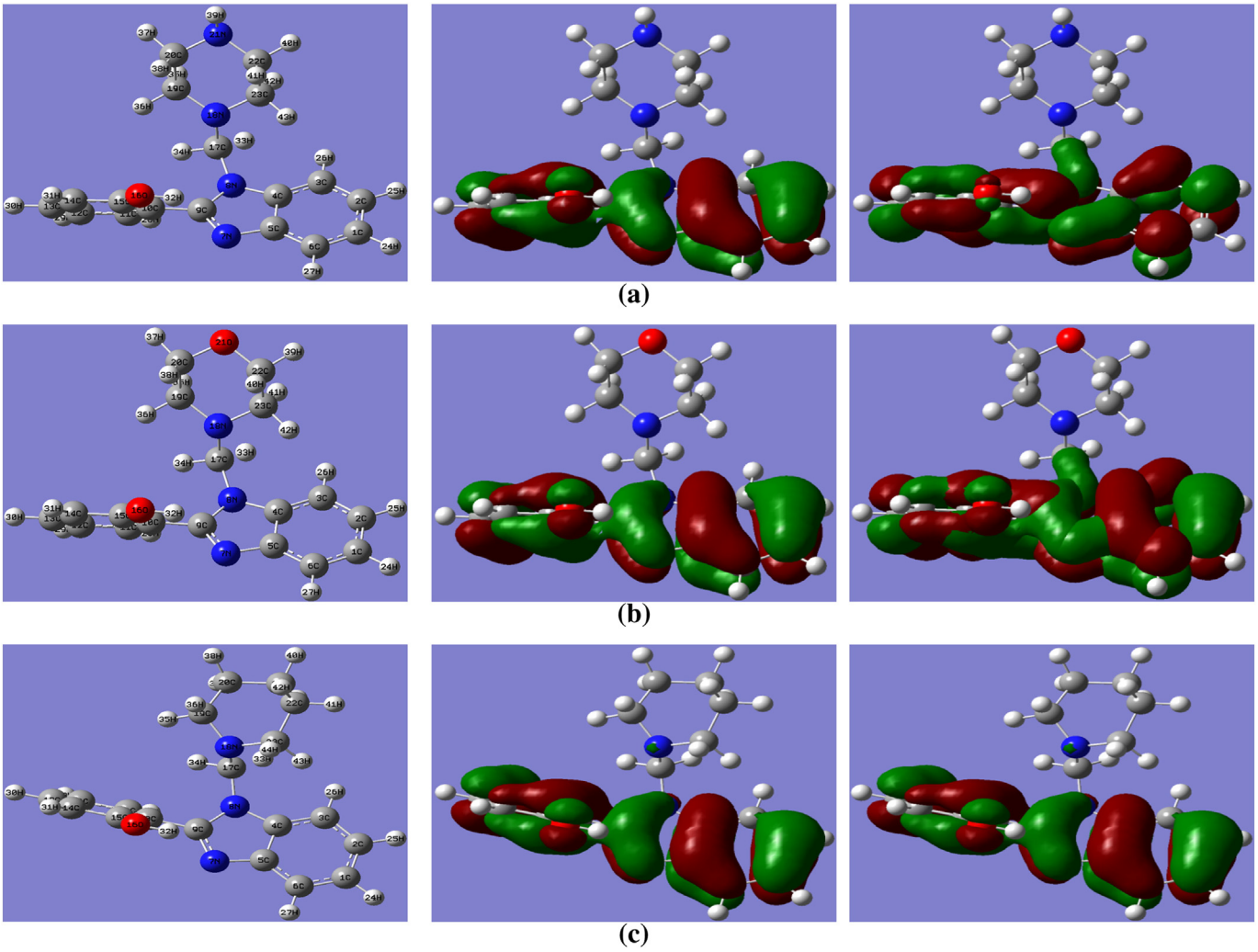

Fig. 13. The optimized structure (left) and HOMO (center) and LUMO (right) distribution for molecules (a) PzMBP, (b) MBP and (c) PMBP. [Atom legend: white = H; Cyan = C; blue = N; red = O]. (For interpretation of the references to color in this figure legend, the reader is referred to the web version of this article.)

from Fig. 14 that all the three inhibitors have considerable excess of negative charge around the nitrogen atoms in the benzoimidazole ring, oxygen of the hydroxyl group and also on some carbon atoms. Large negative Mulliken charges are also found on both nitrogen atoms of piperazine ring, nitrogen of piperidine as well as nitrogen and oxygen of morpholine ring. This suggests that these centers are the coordinating sites through which the inhibitors will adsorb on a positively charged metal surface.

All quantum chemical parameters were derived from the electronic data of the corresponding optimized structures. The frontier molecular orbital (FMO) energies (E_{HOMO} and E_{LUMO}) are significant parameters for the prediction of the reactivity of a chemical species. The E_{HOMO} is often associated with the electron donating ability of a molecule. High E_{HOMO} values indicate that the molecule has a high tendency to donate electrons to appropriate acceptor molecules with low energy empty molecular orbitals. The lower value of E_{LUMO} for a molecule suggests that the molecule can readily accept electrons from the donor molecules [44]. It has also been reported that smaller values of ΔE and higher values of dipole moment (μ) favor higher inhibition efficiency [45]. Global hardness (η) and softness (σ) are another parameters used to assess the reactivity of molecules. According to hard and soft acid/base (HSAB) theory, hard acids prefer to co-ordinate to hard bases and soft acid to soft bases. Fe is considered as soft acid and will co-ordinate to molecule having maximum softness and small energy gap ($\Delta E = E_{LUMO} - E_{HOMO}$). Soft molecules are considered to be more reactive than hard ones because they can offer electron to acceptors easily [46]. The global electronegativity (χ), η and σ were calculated according to the equations [45]:

$$\chi = -\frac{E_{LUMO} + E_{HOMO}}{2} \tag{11}$$

$$\eta = \frac{E_{LUMO} - E_{HOMO}}{2} \tag{12}$$

$$\sigma = \frac{1}{\eta} \tag{13}$$

and the results are reported in Table 6. Kokalj recently reported [47] that the work function (Φ) of a metal surface is an appropriate measure of its electronegativity and should be used together with its vanishing absolute hardness to estimate the fraction of electrons transferred (ΔN) as

$$\Delta N = \frac{\Phi - \chi_{inh}}{2\eta_{inh}} = \frac{\chi_{Fe} - \chi_{inh}}{2(\eta_{Fe} + \eta_{inh})} \tag{14}$$

where the electronegativity of Fe, $\chi_{Fe} \approx 7$ eV mol^{-1} and the global hardness of bulk iron, $\eta_{Fe} = 0$ eV mol^{-1}.

From the results in Table 6 it is clear that the highest value of E_{HOMO} (-5.226 eV), σ (0.521), ΔN (0.96) and lowest values of ΔE (3.842 eV) were found for PzMBP, indicating that PzMBP has more potency to get

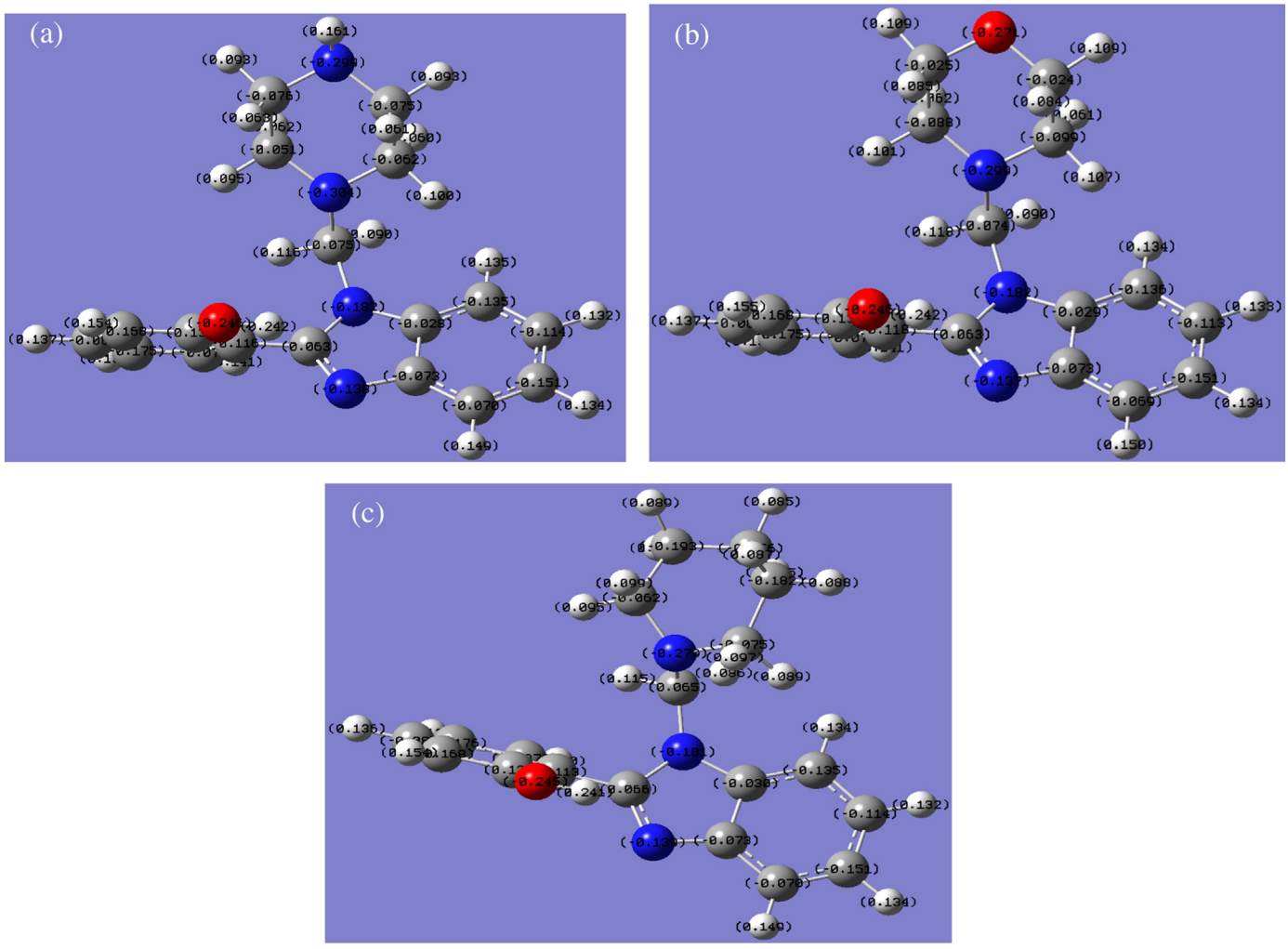

Fig. 14. The Mulliken charge density of (a) PzMBP, (b) MBP and (c) PMBP.

adsorbed on the N80 steel surface resulting in greater inhibition tendency than MBP and PMBP. The high dipole moments of these molecules suggest that the inhibitors are polar compounds and can easily get adsorbed on metal surface in aqueous solutions to form strong dπ–pπ bonding [48]. The dipole moment of the studied compounds is in the order PzMBP (5.256 D) > MBP (4.783 D) > PMBP (4.358 D) which agrees with the trend of the experimentally determined η%. This observation implies that high polarity of the inhibitor molecules will facilitate electrostatic interactions between the electric field of the charged metal surface and the electric moments of the inhibitor molecules thereby enhance surface adsorption by influencing the transport process through the adsorbed layer [49].

The value of ΔN is used as a gauge of the fraction of electrons transferred from the inhibitor molecule to the iron atom and it is used to predict the mode of electron donation (forward or backward) that results in increase in inhibition efficiency of the inhibitors. According to Lukovits et al. [50] if the value of ΔN is less than 3.6, the inhibition efficiency of the inhibitor increases with increasing electron-donating ability of the inhibitor at the metal surface. The structure of PzMBP, MBP and PMBP are almost similar only the difference is that PzMBP contains piperazine ring, MBP contains morpholine ring whereas PMBP contains piperidine ring. The electronic-releasing power of PzMBP was found to be better than MBP due to higher basicity of piperazine ring nitrogen compared to morpholine ring oxygen and hence improved the inhibition efficiency of PzMBP. PMBP shows lowest electron-releasing power because it has no free heteroatom except nitrogen to share its lone pair of electrons with iron. In this study, it can be seen from Table 6 that the trend of ΔN follows the order PzMBP > MBP > PMBP, which is in good agreement with the order experimental η% values.

Table 6
Quantum chemical parameters for different inhibitors.

Inhibitor	E_{HOMO} (eV)	E_{LUMO} (eV)	ΔE (eV)	μ (D)	γ (eV)	σ (eV^{-1})	χ	ΔN (e)
PzMBP	−5.226	−1.378	3.842	5.256	1.921	0.521	3.302	0.96
MBP	−5.468	−1.336	4.132	4.783	2.066	0.484	3.402	0.87
PMBP	−5.625	−1.312	4.313	4.358	2.157	0.464	3.469	0.81

3.9. Mechanism of inhibition

The inhibition of N80 steel corrosion in 15% HCl solution by the studied inhibitors: PzMBP, MBP and PMBP can be explained on the basis of molecular adsorption. These compounds inhibit corrosion by controlling both anodic as well as cathodic reactions. It has been reported in literature that inhibitors with donor atoms and highly basic sites can be protonated in acidic solutions [51]. The nitrogen atoms present in the studied inhibitors can readily be protonated in acidic solution to form quaternary compounds. These protonated species adsorbed can adsorb on the cathodic sites of the N80 steel and decrease the evolution of hydrogen. The adsorption on anodic site may occur through π-electrons of aromatic rings and lone pair of electrons of nitrogen and oxygen atoms leading to the decrease in anodic dissolution of N80 steel. The inhibitors PzMBP, MBP and PMBP are expected to get adsorbed through the lone

pairs of electrons on N atoms of benzimidazole ring, —C═N group, N atoms of piperazine and piperidine, nitrogen and oxygen of morpholine ring, hydroxyl oxygen atom and delocalized π-electron density on benzimidazole and phenyl rings by their coordination with N80 steel surface.

4. Conclusions

Three benzimidazole derivatives PzMBP, MBP and PMBP have been synthesized, characterized and assessed for their corrosion inhibition potentials on N80 steel in 15% HCl solution. The following conclusions can be drawn from the studies.

* The synthesized benzimidazole derivatives show good inhibition efficiencies for the corrosion of N80 steel in 15% HCl solutions and the inhibition efficiency increases on increasing concentration of the inhibitors and decreases with increase in temperature. The order of the inhibition efficiency is: PzMBP > MBP > PMBP.
* The variation in the values of β_a and β_c (Tafel slopes) and the minor displacement of E_{corr} with respect to E_{corr} of the blank indicate that all the three inhibitors are mixed type in nature.
* EIS measurements show that the charge transfer resistance (R_{ct}) increases and the double layer capacitance (C_{dl}) decreases in the presence of the inhibitors which implied the adsorption of the inhibitor molecules on the N80 steel surface.
* The FTIR and UV–vis spectra established the interactions between the inhibitors and N80 steel and the possible formation of Fe/inhibitor complex, while SEM and AFM images confirmed the adsorption of the inhibitors on the steel surface.
* The adsorption of the inhibitors was found to be spontaneous and obey the Langmuir adsorption isotherm featuring competitive physisorption and chemisorption mechanisms.
* Quantum chemical calculations showed a good agreement between the theoretical and experimental results.

Acknowledgments

The authors acknowledge the funding from North-West University and Department of Science and Technology and the National Research Foundation (DST/NRF) South Africa grant funded (Grant UID: 92333) for the postdoctoral scholarship of Dr. I. Bahadur.

References

[1] K.D. Neemla, A. Jayaraman, R.C. Saxena, A.K. Agrawal, R. Krishna, Bull. Electrochem. 5 (1989) 250–253.
[2] M.A. Quraishi, N. Sardar, H. Ali, Corrosion 58 (2002) 317–321.
[3] S. Vishwanatham, P.K. Sinha, Anti-Corros. Methods Mater. 56 (2009) 139–144.
[4] E.T. Kumar, S. Vishawanatam, G. Udaybhanu, Corros. Eng. Sci. Technol. 39 (2004) 327–332.
[5] M. Yadav, D. Behera, U. Sharma, Corros. Eng. Sci. Technol. 48 (2013) 19–27.
[6] M. Yadav, D. Behera, U. Sharma, Arab. J. Chem. DOI/http://dx.doi.org/10.1016/j.arabjc.2012.03.011.
[7] M. Yadav, U. Sharma, J. Mater. Environ. Sci. 2 (2011) 407–414.
[8] S. Kumar, D. Sharma, P.N. Yadav, M. Yadav, Ind. Eng. Chem. Res. 52 (2013) 14019–14029.
[9] M.M. Singh, S. Banerjee, V. Srivastava, Corros. Sci. 59 (2012) 35–46.
[10] H.L. Wang, H.B. Fan, J.S. Zheng, Mater. Chem. Phys. 77 (2002) 655–661.
[11] S. Tamilselvi, V. Raman, N. Rajendran, J. Appl. Electrochem. 33 (2003) 1175–1182.
[12] Q.B. Zhang, Y.X. Hua, Electrochim. Acta 54 (2009) 1881–1887.
[13] F. Bentiss, M. Lebrini, H. Vezin, M. Lagrenee, Mater. Chem. Phys. 87 (2004) 18–23.
[14] R. Solmaz, G. Kardaş, M. Çulha, B. Yazıcı, M. Erbil, Electrochim. Acta 53 (2008) 5941–5952.
[15] A. Popova, E. Sokolova, S. Raicheva, M. Christov, Corros. Sci. 45 (2003) 33–58.
[16] A. Popova, M. Christov, S. Raicheva, E. Sokolova, Corros. Sci. 46 (2004) 1333–1350.
[17] I. Ahamad, M.A. Quraishi, Corros. Sci. 52 (2010) 651–656.
[18] I. Ahamad, M.A. Quraishi, Corros. Sci. 51 (2009) 2006–2013.
[19] A. Aouniti, R. Mokhlisse, S. Kertit, K. Elkacemi, Ann. Chim. Sci. Mater. 25 (2000) 437–446.
[20] Y. Abboud, A. Abourriche, T. Saffaj, M. Berrada, M. Charrouf, A. Bennamara, A. Cherqaoui, D. Takky, Appl. Surf. Sci. 252 (2006) 8178–8184.
[21] S. Srivastava, S.N. Pandeya, M.K. Yadav, B.K. Singh, J. Chem. 2013 (2013), 694295.
[22] A. Dhanapala, S.R. Boopathy, V. Balasubramanian, J. Alloys. Compd. 523 (2012) 49–60.
[23] M. Özcan, I. Dehri, M. Erbil, Appl. Surf. Sci. 236 (2004) 155–164.
[24] C. Lee, W. Yang, R.G. Parr, Phys. Rev. B 37 (1988) 785–789.
[25] A.D. Becke, J. Chem. Phys. 98 (1993) 1372–1377.
[26] S.S. Abdel-Rehim, M.A.M. Ibrahim, K.F. Khaled, J. Appl. Electrochem. 29 (1999) 593–599.
[27] A.U. Ezeoke, O.G. Adeyemi, O.A. Akerele, N.O. Obi-Egbedi, Int. J. Electrochem. Sci. 7 (2012) 534–553.
[28] L. Fragoza-Mar, O. Olivares-Xometl, M.A. Domínguez-Aguilar, E.A. Flores, P. Arellanes-Lozada, F. Jimenez-Cruz, Corros. Sci. 61 (2012) 171–184.
[29] İ. Dehri, M. Özcan, Mater. Chem. Phys. 98 (2006) 316–323.
[30] E.E. Oguzie, Corros. Sci. 50 (2008) 2993–2998.
[31] S.V. Ramesh, V. Adhikari, Bull. Mater. Sci. 31 (2007) 699–709.
[32] M. Behpour, S.M. Ghoreishi, N. Soltani, M. Salavati-Niasari, M. Hamadanian, A. Gandomi, Corros. Sci. 50 (2008) 2172–2181.
[33] S.K. Shukla, M.A. Quraishi, Corros. Sci. 51 (2009) 1990–1997.
[34] M. Ozcan, J. Solid State, Electrochemistry 12 (2008) 1653–1661.
[35] X. Wang, H. Yang, F. Wang, Corros. Sci. 53 (2011) 113–121.
[36] D. Jayaperumal, Mater. Chem. Phys. 119 (2010) 478–484.
[37] E.S. Ferreira, C. Giancomlli, F.C. Giacomlli, A. Spinelli, Mater. Chem. Phys. 83 (2004) 129–134.
[38] S. Ramesh, S. Rajeswari, Electrochim. Acta 49 (2004) 811–820.
[39] H. Ashassi-Sorkhabi, B. Shaabani, D. Seifzadeh, Appl. Surf. Sci. 239 (2005) 154–164.
[40] E.E. Foad, S.M.A. Wahaab, M. Deyab, Mater. Chem. Phys. 89 (2005) 183–191.
[41] F. Kandemirli, S. Sagdinc, Corros. Sci. 49 (2007) 2118–2130.
[42] D.K. Yadav, B. Maiti, M.A. Quraishi, Corros. Sci. 52 (2010) 3586–3598.
[43] R. Hasanov, M. Sadıkoğlu, S. Bilgiç, Appl. Surf. Sci. 253 (2007) 3913–3921.
[44] S. Xia, M. Qiu, L. Yu, F. Liu, H. Zhao, Corros. Sci. 50 (2008) 2021–2029.
[45] Y.M. Tang, W.Z. Yang, X.S. Yin, Y. Liu, R. Wan, J.T. Wang, Mater. Chem. Phys. 116 (2009) 479–483.
[46] V.S. Sastri, J.R. Perumareddi, Corrosion 53 (1997) 617–622.
[47] A. Kokalj, Chem. Phys. 393 (2012) 1–12.
[48] I.B. Obot, N.O. Obi-Egbedi, Mater. Chem. Phys. 122 (2010) 325–328.
[49] K. Babić-Samardžija, K.F. Khaled, N. Hackerman, Appl. Surf. Sci. 240 (2005) 327–340.
[50] I. Lukovits, E. Klaman, F. Zucchi, Corrosion 57 (2001) 3–8.
[51] L.O. Olasunkanmi, I.B. Obot, M.M. Kabanda, E.E. Ebenso, J. Phys. Chem. C (2015), http://dx.doi.org/10.1021/acs.jpcc.5b03285.